Ecological drivers of phytoplankton bloom cycles in the Southern Ocean

Lionel Arteaga[1], Emmanuel Boss[2], Michael Behrenfeld[3], Toby Westberry[3], and Jorge Sarmiento[1]

[1]Princeton University
[2]University of Maine
[3]Oregon State University

November 22, 2022

Abstract

Over the last ten years, satellite and geographically constrained in situ observations largely focused on the northern hemisphere have suggested that annual phytoplankton biomass cycles in bloom-forming ocean regions cannot be fully understood from environmental properties controlling phytoplankton division rates (e.g., nutrients and light). Here, we use multi-year observations from a very large array of robotic drifting buoys in the Southern Ocean to determine key factors governing phytoplankton biomass dynamics over the annual cycle. Our analysis reveals phytoplankton blooming events occurring during periods of declining division rates, an observation that clearly highlights the importance of changing loss processes in dictating the evolution of the bloom. Bloom magnitude is found to be greatest in areas with high dissolved iron concentrations, consistent with iron being a well-established primary limiting nutrient in the Southern Ocean. Projections for expected future seasonal variations in nutrient and light availability indicate a 10% change in phytoplankton division rate may be associated with a 50% reduction in mean bloom magnitude and annual primary productivity in the Southern Ocean. Our results highlight the importance of quantifying and accounting for both changing phytoplankton division and loss processes when modeling future changes in phytoplankton bloom cycles.

1

Ecological drivers of phytoplankton bloom cycles in the Southern Ocean

Lionel A. Arteaga[1*], Emmanuel Boss [2], Michael J. Behrenfeld [3], Toby Westberry [3], Jorge L. Sarmiento [1]

(*) Corresponding author

Afiliations:

- (1) Program in Atmospheric and Oceanic Sciences, Princeton University, 300 Forrestal Rd, Princeton, NJ, USA,

- (2) School of Marine Sciences, 5706 Aubert Hall, University of Maine, Orono, Maine 04469−5741, USA.

- (3) Department of Botany and Plant Pathology, Cordley Hall 2082, Oregon State University, Corvallis, Oregon 97331−2902, USA.

Abstract

Over the last ten years, satellite and geographically constrained in situ observations largely focused on the northern hemisphere have suggested that annual phytoplankton biomass cycles in bloom-forming ocean regions cannot be fully understood from environmental properties controlling phytoplankton division rates (e.g., nutrients and light). Here, we use multi-year observations from a very large array of robotic drifting buoys in the Southern Ocean to determine key factors governing phytoplankton biomass dynamics over the annual cycle. Our analysis reveals phytoplankton blooming events occurring during periods of declining division rates, an observation that clearly highlights the importance of changing loss processes in dictating the evolution of the bloom. Bloom magnitude is found to be greatest in areas with high dissolved iron concentrations, consistent with iron being a well-established primary limiting nutrient

in the Southern Ocean. Projections for expected future seasonal variations in nutrient and light availability indicate a 10% change in phytoplankton division rate may be associated with a 50% reduction in mean bloom magnitude and annual primary productivity in the Southern Ocean. Our results highlight the importance of quantifying and accounting for both changing phytoplankton division and loss processes when modeling future changes in phytoplankton bloom cycles.

The photosynthetic production of organic carbon by marine phytoplankton plays a key role in regulating atmospheric carbon dioxide (CO_2) levels, such that without this biological uptake it is estimated that present day atmospheric CO_2 concentrations would be 200 ppm (50%) higher[1]. Phytoplankton blooms in the temperate and polar oceans play a disproportionally large role in ocean CO_2 uptake, as well as being critical ecological events to which the migration patterns of marine animals, ranging from zooplankton to whales, have evolved[2]. The cause of phytoplankton blooms has traditionally been attributed to seasonal changes in 'bottom-up' environmental factors controlling phytoplankton division rates, such as nutrients and light[3,4,5,6,7]. However, seasonal changes in phytoplankton biomass (r) always reflect the interplay between two dominant terms, the phytoplankton division rate (μ) and the sum of all loss (l) rates (e.g., grazing, viruses, sinking):

$$r = \mu - l \tag{1}$$

implying that a 'bottom-up' interpretation of blooms is, by necessity, incomplete[8,9,10]. The importance of seasonal variations in loss rates has recently been highlighted by satellite and in situ studies demonstrating that annual blooming events often begin in early winter when phytoplankton division rates are still declining[11,12,13,10,14,15], but these earlier investigations have largely focused on regions of the northern hemisphere. Here, we use multi-year in-situ bio-optical measurements from 146 robotic drifting buoys (floats) in the Southern

Ocean (south of 30°S), in conjunction with satellite data, to resolve ecological drivers of phytoplankton biomass cycles. Our results demonstrate a closely-coupled interplay between 'bottom-up' and 'top-down' (i.e., loss) processes controlling the onset and temporal evolution of Southern Ocean blooms. Integrating this finding into a productivity model indicates that small changes in phytoplankton division rates associated with predicted changes in Southern Ocean environmental conditions may result in disproportionately large decreases in future bloom magnitude and primary production.

Bloom cycles in the Southern Ocean

For the current analysis, we used float measurements collected between March 6, 2012 and March 12, 2019, which provided broad coverage of the Southern Ocean region (Figure S1). Annual cycles of phytoplankton biomass were obtained from empirical relationships between float-measured particulate backscatter coefficients at 700 nm ($b_{bp}(700)$) and phytoplankton carbon (Methods). These data show that average phytoplankton biomass for the Southern Ocean as a whole is highest (~ 900 mg C m^{-2}) during austral summer (January – February) (Figure 1) and exhibits a seasonal cycle correlated with the shoaling and deepening of the mixed layer, the average light level within the mixed layer, and seasonal changes in phytoplankton division rates (Methods). Interestingly, phytoplankton division rates (μ) are about 2 – 3 months time-lagged behind net accumulation rates (r), a clear indication that seasonal changes in biomass are not exclusively driven by 'bottom-up' factors. Moreover, values of r are ~ 100 times lower than μ, indicating that growth and loss processes must be tightly coupled and of similar magnitude.

Initiation of the blooming period (BI) can be identified by a negative-to-positive change in sign of the accumulation rate, r . In the four annual cycles of biomass analyzed between 2015 and 2019, BI occurs at the end of winter when incident sunlight is lowest, phytoplankton division rates are minimal, and mixing is deepest. Also counterintuitively, bloom termination

72 (BT), marked by a positive-to-negative sign change in r, occurs when phytoplankton division

73 rates are near-maximal. The temporal misalignment between division rate (μ) and accumu-

74 lation rates (r) can only be explained by subtle seasonal changes in the balance between μ

75 and loss (l) rates.

76 Additional insight on processes affecting bloom phenology is provided by changes in

77 the temporal gradient (slope) of r. The moment when r stops decreasing (but is still <

78 0) marks the time in autumn when the rate of biomass decline starts decelerating (DD,

79 Figure 1). This event begins in early winter while conditions for phytoplankton growth are

80 still deteriorating, but the rate of decrease in μ begins to slow (Figure 1c). These findings

81 imply that the rate of change in phytoplankton biomass is not dependent on the absolute

82 value of μ, but rather on the rate of change in μ. Such a relationship will exist when

83 division and loss rates are tightly coupled, but a temporal lag exists in the response time for

84 the loss processes[16,15,10]. During the autumn-to-winter transition, an additional important

85 factor influencing the balance between phytoplankton division and loss rates is the transient

86 dilution effect caused by a deepening mixed layer, which reduces phytoplankton mortality

87 through a decrease in the predator-prey encounter rates[11,8,17].

88 Even when integrated over our full Southern Ocean domain, the extensive float record

89 analyzed here immediately highlights the important role of predator-prey relationships in

90 terms of governing the annual phytoplankton biomass cycle. The Southern Ocean, how-

91 ever, is comprised of well-established and distinct environmental zones that can provide

92 more detailed understanding of biomass variability (Figure S1). We therefore subdivided

93 the Southern Ocean into four primary zones of differing physical and biogeochemical char-

94 acteristics (Methods): a Subtropical Zone (STZ) roughly encompassing oligotrophic waters

95 between 30°S and 40°S, a Subantarctic Zone (SAZ) and a Polar Antarctic Zone (PAZ) that

96 together cover the circumpolar section between approximately 40°S and 60°S, and a Sea-

97 sonal Ice Zone (SIZ) representing seasonally ice-covered areas between Antarctica and $\sim$

4

60°S. For each zone, we evaluated seasonal patterns in phytoplankton biomass to identify key mechanisms driving variations in biomass accumulation rates.

Subantarctic and Polar Antarctic Zones

The SAZ and PAZ show similar annual cycles of r, with bloom initiation (at the beginning of the blooming phase) occurring in July and corresponding to near-minimal phytoplankton division rates (Figure 2). As observed for the integrated Southern Ocean (Figure 1), peak values of μ for the SAZ and PAZ occur approximately 3 months after the annual peak in accumulation rate (r). In contrast, the annual cycle in r is temporally aligned with that of the division rate of change ($d\mu/dt$, i.e., the temporal derivative of μ). Satellite observations of the polar zones earlier revealed $d\mu/dt$ as a principal driver of variation in phytoplankton concentration[15]. The interpretation of this finding has been that accelerations in μ result in an accumulation of biomass because they allow phytoplankton division to outpace growing loss rates, whereas decelerations in μ result in overgrazing and thus declining biomass. In this view of annual phytoplankton cycles, the importance of 'bottom-up' factors resides in their influence on 'top-down' predator-prey relations and, for the Southern Ocean, plays out in synchrony with seasonal changes mixed layer light levels (Figure 1).

In addition to the dominant spring bloom, the SAZ also exhibits a less-pronounced autumn bloom that corresponds to the initial deepening of the mixed layer. One potential explanation for this feature is that it reflects an entrainment of deeper phytoplankton populations into the mixed layer, but analysis of our float time-series data rarely showed the enhanced deep-water biomass prior to mixed layer deepening that would be necessary to support this explanation. Alternatively, autumn mixing could be envisioned to enhance mixed layer nutrient concentrations and thus stimulate blooming, but this interpretation is not supported by estimated division rates during this period (Figure 2), noting however that our phytoplankton growth model does not explicitly resolve unique attributes of iron stress

5

123 (Methods)[18]. A direct physical trigger for the SAZ autumn blooms may be the primary
124 driver of this event, where deepening of the mixed layer dilutes the plankton populations
125 and consequently relaxes phytoplankton mortality rates[11,8,17].

Subtropical and Seasonal Ice Zones

127 The STZ and SIZ represent extreme conditions for the Southern Ocean in terms of their
128 latitudinal location, biogeochemical properties (Figure S1), and contrasting cycles in biomass
129 accumulation rates (Figure 3). In the STZ, the annual cycle of r is counterintuitively a
130 near mirror image of the annual cycle in μ (Figure 3a), with the blooming phase taking
131 place during months with the lowest mixed layer light levels. What this finding suggests
132 is accelerations and decelerations in division rate are not the dominant driver of biomass
133 variability. What we instead find is that accumulation rates in the STZ covary with the rate
134 of change in mixed layer depth (dMLD/dt). Thus, the blooming phase ($r > 0$) generally
135 coincides with periods of mixed layer deepening (dMLD/dt > 0) and the period of declining
136 biomass corresponds to mixed layer shoaling (dMLD/dt < 0). This pattern suggests a
137 dominant role for the physical impacts of mixing, where deepening of the mixed layer causes
138 a reduction in light-limited phytoplankton division rates but and even greater decrease in loss
139 (grazing) rates due to the dilution effect discussed above[11,19]. Seasonal changes in mixed layer
140 nutrient availability might also be envisioned as contributing to the unique annual cycle of r
141 for the STZ. However, mixed layer nitrate remains above limiting levels ($> 1 \ \mu$mol kg^{-1})[20]
142 throughout the year (Figure S2) and, of our four Southern Ocean zones, the STZ is least
143 associated with iron limiting conditions[21], with mean dissolved iron concentrations remaining
144 above > 0.2 nmol kg^{-1} (Figure S2). These observations imply that winter enhancements and
145 summer depletion of nutrients likely do not contribute significantly to the unique seasonal
146 cycle in r for the STZ.

147 Floats used in this study were equipped with ice avoidance software[22], enabling water

column sampling beneath ice and thus providing observations throughout the year in the SIZ[23] (Figure 3b). Seasonal cycles in phytoplankton division (μ) and accumulation (r) rates are similar in the SIZ, with no evident time lag between the two properties. Importantly, under-ice observations in this region documented initiation of the blooming phase prior to ice-out (around September), a phenomenon that has not been accessible through earlier satellite studies of bloom dynamics. Here we define under-ice conditions as times when at least 50% of the float data are from profiles below ice (> 30 under-ice profiles per week between June and September for the combined period between 2012 and 2019). Under-ice blooming has been observed at local scales in the Arctic[24] and near Antarctica[25], but our geographically extensive float data set demonstrates that this phenomenon is a common feature of the SIZ. What makes this event particularly remarkable is the low light level at which blooming appears to begin. Specifically, winter mixed layer light levels in the SIZ are estimated here at $< 1 \, \mathrm{E} \, \mathrm{m}^{-2} \, \mathrm{d}^{-1}$ (Figure S3) and these values do not include the albedo effect of ice which could reduce these estimates to values close to the compensation level where phytoplankton photosynthesis only supports cellular respiration $\sim 0.04 \, \mathrm{E} \, \mathrm{m}^{-2} \, \mathrm{d}^{-1}$,[26]. Such extreme mixed layer light-limiting conditions only exist in very high polar latitudes such as the SIZ[10] and may explain the tight temporal coupling between r and μ (i.e., impeding even earlier bloom initiation) observed in this zone exclusively.

Projected changes in phytoplankton bloom seasonality and magnitude

Light limitation is the dominant factor controlling phytoplankton division in the Southern Ocean, explaining 66% (p-value < 0.05) of the variability in division rates (μ) (Figure 4a). However, the magnitude of blooms in the region (i.e., the difference between the mean winter and summer phytoplankton biomass) is correlated with mean surface dissolved iron concentration (Figure 4b). This finding is in line with the well known constraint of iron limitation on biological productivity in the Southern Ocean[27,28,21]. Future changes in surface

7

iron availability could thus alter the magnitude of Southern Ocean bloom cycles with respect to present conditions, with implications for marine carbon productivity and export.

Current projections suggest that the Southern Ocean will generally experience an increase in surface ocean stratification in the future[29]. Associated with this intensified stratification will likely be an increase in summer nutrient limitation and a relaxation of winter light limitation[30]. We assessed the sensitivity of the annual cycle in phytoplankton biomass in the Southern Ocean to changes in the division rates by increasing and decreasing μ over a range from 10% to 60% with respect to current values during winter and summer, respectively. For these simulations, we assumed that loss rates paralleled changes in μ but with a temporal lag[10] (Methods). We find that environmental changes that lead to a decrease in summer division rates tend to reduce bloom magnitude and mean annual productivity despite increased μ during winter (Figure 4c, 4d, and S7). Specifically, bloom magnitude decreases from a mean of 12 mg C m^{-3} for present conditions to 6 mg C m^{-3} for a 10% change in μ and to $\sim$ 2 mg C m^{-3} for a 60% change in μ. Similarly, annual mean vertically integrated net primary production (NPP) decreases from 324 mg C m^{-2} d^{-1} for present conditions to 181 mg C m^{-2} d^{-1} and 56 mg C m^{-2} d^{-1} for 10% and 60% changes in μ, respectively. Thus, even a 10% change in μ results in a surprising 50% reduction in bloom magnitude and NPP. While the impact of such changes on oceanic carbon export and sequestration remains to be quantified, our analysis suggests that relatively small changes in phytoplankton division rates in the Southern Ocean could result in flatter seasonal biomass cycles that more closely resemble current lower latitude regions.

Future perspectives on phytoplankton bloom cycles

Over the last ten years, satellite and limited in situ studies have shown that phytoplankton biomass often starts increasing in early winter and prior to surface mixed layer shoaling, a finding inconsistent with the classical light-driven interpretation of blooms[12,11,13,10,14,15]. A

8

new 'Disturbance-Recovery' hypothesis has been proposed that accommodates these findings, where disturbances such as mixed layer deepening impact predator-prey relationships and seasonal accelerations and decelerations in division rate drive changes in phytoplankton concentration over the annual cycle. Development of this hypothesis has largely been based on observation in the northern hemisphere and strongly biased toward satellite, rather than in situ, data. Here, a large array of biogeochemical floats deployed over the last 7 years has allowed a detailed and in situ evaluation of phytoplankton bloom dynamics in the Southern Ocean. For the region as a whole and for the four subregions investigated, we find that seasonal variations in phytoplankton biomass are well accounted for by the fundamental mechanisms encompassed by the 'Disturbance-Recovery' hypothesis. However, we also find that the relative importance of disturbances (i.e., dilution of plankton populations by mixed layer deepening) versus accelerations and decelerations in division rate differs between Southern Ocean zones.

Among high latitude regions, the Southern Ocean has major biogeochemical significance, with strong air-sea CO_2 fluxes[31,32] and a nutrient supply fueling global marine biological productivity north of $30°S$[33]. Understanding the biological engine of the Southern Ocean, and more specifically phytoplankton accumulation and decay cycles (blooms), is therefore key to quantifying biogeochemical fluxes and projecting future changes in marine planktonic ecosystems. In the context of the 'Disturbance-Recovery' hypothesis, our findings emphasize the important interplay between 'bottom-up' and 'top-down' process and suggest that large changes in carbon biogeochemistry can result from relatively small changes in mixed layer growth conditions. Continued efforts to better quantify loss rates could provide powerful insights on our understanding of biomass cycles, particularly for discerning the relative role of winter dilution versus nutrient fertilization in regions where the blooming phase is aligned with a deepening of the surface mixed layer. Equipping biogeochemical floats with light sensors would provide both complementary data for comparison with remote sensing data

9

and a unique perspective of the submarine light field experienced by polar phytoplankton under ice. Finally, a refocus in modeling efforts is needed to develop more realistic simulations of both autotroph and heterotroph responses to changes in the physical environment [19,10,34] in order to project with fidelity future changes in phytoplankton phenology and bloom intensity that depart from the current ecological mean state.

Methods

Float data

Quality-controlled float data analyzed in this study was downloaded from the Southern Ocean Carbon and Climate Observations and Modeling (SOCCOM) data portal (`http://soccompu.princeton.edu/www/index.html`). The SOCCOM program is focused on understanding the carbon cycle in the Southern Ocean and determining its influence on climate through the deployment of biogeochemical (BGC)-Argo floats and state-of-the-art climate models. We obtained the latest (March, 12, 2019) low resolution data snapshot (with LIAR-based estimation of carbon chemistry variables, not used) published as a MATLAB data file[35]. The floats are equipped with a CTD (conductivity-temperature-depth), oxygen, nitrate, pH and bio-optical sensors (fluorescence and particulate backscattering at 700 nm ($b_{bp}(700)$))[23]. SOCCOM BGC-Argo floats sample the vertical water column every 10 or 5 days, depending on the preset programming of the float, with most floats sampling every 10 days. The vertical resolution of the measurements taken by the floats varies with depth, with measurements every 5 m in the upper 100 m. The uppermost sampled depth is $\sim$ 5 or 7 m below surface. Vertical sampling resolution decreases to 10 m below 100 m depth, 20 m below 360 m depth, and 50 m between 400 and 2000 m depth. Vertical profiles are smoothed using a seven point running-median filter. Float data corresponds to the period from 06/Mar/2012 to 12/Mar/2019. For multi-annual time series of the entire Southern Ocean (Figure 1), we focused on the period from January 2015 onwards, which has a sufficient profiles to permit complete representation of all ocean basins south of 30°S. All analyses presented were conducted using the scientific programming software MATLAB (version 2017a).

11

Estimates of phytoplankton carbon and chlorophyll

Estimates of particulate organic carbon (POC, mg m^{-3}) are obtained based on an empirical relationship established between POC samples taken during float deployment and float measured $b_{\mathrm{bp}}(700)$ [23,36]:

$$\mathrm{POC} = 3.12 \times 10^4 (\pm 2.47 \times 10^3) \times b_{\mathrm{bp}}(700) + 3.0(\pm 6.8) \tag{2}$$

Phytoplankton carbon (C$_{\mathrm{phyto}}$, mg m^{-3}) is estimated from an empirical relationship with POC[37] uncertainties of the empirical relationship are not provided:

$$\mathrm{C_{phyto}} = 0.19 \times \mathrm{POC} \pm 8.7 \tag{3}$$

Chlorophyll concentration (Chl, mg m^{-3}) is obtained from float fluorescence measurements corrected for non-photochemical quenching (NPQ) and calibrated against High Performance Liquid Chromatography (HPLC) measurements based on chlorophyll samples taken during SOCCOM float deployments details in [23,36]. Float estimates of POC and Chl agree well with satellite ocean color retrievals for the Southern Ocean[36]. For each C$_{\mathrm{phyto}}$ profile we subtract the mean estimated concentration between 900 m and 2000 m from the entire vertical profile, in order to make sure that phytoplankton carbon asymptotes towards zero at depth. Resulting negative C$_{\mathrm{phyto}}$ concentrations from this subtraction are $\approx$ 2 % in the entire data set, and < 0.001 % in the upper 200 m. Negative Chl estimates represent < 0.01 % of the entire float data set. Negative C$_{\mathrm{phyto}}$ and Chl estimates are ultimately removed in order to avoid spurious outputs from the phytoplankton growth model.

Net accumulation rate

269 The net accumulation rate of phytoplankton biomass (r, d^{-1}) for each float is computed

270 between observational time-points (profiles) using centered-differences[12]:

$$r(t + \frac{\Delta t}{2}) \equiv \begin{cases} \frac{1}{\overline{P}}\frac{d\overline{P}}{dt} \approx \frac{2}{\Delta t}\frac{(\overline{P}(t+\Delta t)-\overline{P}(t))}{(\overline{P}(t+\Delta t)+\overline{P}(t))}, & \text{if } \frac{d\text{MLD}}{dt} < 0 \\ \frac{1}{\int P}\frac{d\int P}{dt} \approx \frac{2}{\Delta t}\frac{(\int P(t+\Delta t)-\int P(t))}{(\int P(t+\Delta t)+\int P(t))}, & \text{otherwise} \end{cases} \tag{4}$$

271 where t is time, $\overline{P}$ is mean C_{phyto} in the mixed layer, and $\int P$ is C_{phyto} integrated from

272 surface to the bottom of the mixed layer. Equation 4 describes a switching algorithm where

273 r is computed from changes in phytoplankton concentration during periods of mixed layer

274 shoaling and from changes in phytoplankton inventory during periods of mixed layer deep-

275 ening (or stationary). The aim of Equation 4 is to remove variations in r not caused by

276 the ecological balance between phytoplankton division rates and losses due to gravitational

277 particle sinking, grazing, or viral infection. Therefore, our accumulation rate estimates high-

278 light biomass variations driven mainly by ecological processes affecting the accumulation

279 and depletion of phytoplankton. Estimates of r based only on $\overline{P}$ will indicate a decrease in

280 net biomass accumulation during periods of plankton dilution due to mixed layer deepening.

281 Estimates based on $\int P$ alone will indicate a decrease in biomass during periods of mixed

282 layer shoaling due to changes in the vertically integrated water layer. While the overall

283 seasonality of r estimates based exclusively on $\overline{P}$ or $\int P$ is similar (Figure S4), differences

284 between $\overline{P}$-based and $\int P$-based estimates of r are observed during mixed layer shoaling and

285 deepening, consistent with the mechanisms explained above (Figure S5) see[12,38] for more

286 details on this methodology. Mixed layer depth estimates are obtained using float in situ

287 temperature and salinity profiles[39].

PAR data

Estimates of cloud-corrected surface ocean photosynthetically available radiation (PAR, E m^{-2} d^{-1}) are obtained form satellite data downloaded from the NASA Ocean Color website (`https://oceancolor.gsfc.nasa.gov`). Daily global maps of MODIS-Aqua PAR (L3, 4km) are obtained for the period between the first and last available float profile (06/Mar/2012 and 12/Mar/2019, respectively). Satellite matchups to float profiles are obtained for the same day and the closest pixel to the spatial position of each float profile. If no satellite data is available, NaN is assigned to the corresponding profile PAR matchup. Under ice profiles with unknown location are also assigned NaN as PAR data matchup. Overall, 77 % of float profiles have a valid assigned PAR matchup.

Dissolved iron data

Information of dissolved iron (Fe, nmol kg^{-1}) is obtained from an updated (June, 2015) version of a global database of dissolved iron observations[40] available at `https://www.bodc.ac.uk/geotraces/data/historical/`. Iron observations are scarce and not gridded. Scattered Fe observations are subsampled by averaging all available observations in the upper 200 m proximate to each float profile within a horizontal radius of 500 m, and taken during the same month as the corresponding float profile.

Bloom magnitude

The bloom magnitude is calculated as the difference between the mean winter (May – July) and summer (November – January) concentration of phytoplankton carbon for each float time series.

14

Phytoplankton growth model

The growth model used here is a modification of the Carbon-based Productivity Model CbPM[41]. The CbPM was originally designed to infer vertical profiles of phytoplankton chlorophyll, carbon, division rates and net primary productivity based on satellite estimates of chlorophyll, phytoplankton carbon, and PAR for the surface ocean. We modified the CbPM in order to estimate vertical profiles of phytoplankton division rates (μ, d^{-1}) based on float vertical profiles of Chl, C_{phyto}, and surface PAR. The underwater light field is depth- and spectrally-resolved based on satellite surface PAR, float Chl information, and constant spectral fractions from an atmospheric radiative transfer model[42]. The phytoplankton division rate is estimated based on the maximum potential division rate $\mu_{max} \approx 2$,[43] a nutrient limitation (saturation) term (index) (NSI) constrained by the local Chl:C ratio, and a light limitation (saturation) term (index) (LSI):

$$\mu = \mu_{max} \times \text{NSI} \times \text{LSI} \tag{5}$$

The NSI is inferred from the relative difference between the actual local Chl:C ratio, the Chl:C value when $\mu = 0$ Chl:$C_{\mu=0} = 0.0003$,[41] and the theoretical maximum Chl:C achieved under replete nutrient conditions at the local light level (Chl:C_{max})[41,44]:

$$\text{NSI} = \frac{\text{Chl:C} - \text{Chl:C}_{\mu=0}}{\text{Chl:C}_{max} - \text{Chl:C}_{\mu=0}} \tag{6}$$

The nutrient saturation/limitation term is driven by variations of the phytoplankton Chl:C ratio, which is expected to be acclimated to the environmental nutrient and light conditions[45,46]. The model was primarily conceived to diagnose nutrient limitation caused by nitrate depravation[44,41]. Since biological productivity in the Southern Ocean is considered to be iron limited[27,28,21], an important caveat of the growth model used here is that it is

15

329 not clear how well can the Chl:C ratio represent physiological effects of iron limitation on
330 phytoplankton growth. To a certain degree, iron deprivation should reduce phytoplankton
331 division rates and Chl synthesis, leading to a reduction of Chl:C[47]. Hence, we expect that
332 physiological changes in Chl:C can also serve as an indicator for iron limitation.

333   The LSI is constrained by the local light level at each depth (z)

$$\text{LSI} = 1 - e^{(-5\text{PAR}(z))} \tag{7}$$

Time series smoothing

335 Annual cycles of integrated biomass, mean mixed layer light and depth, as well as r and μ
336 for the Southern Ocean are produced by sorting in time all available float-based estimates
337 between 2015 and 2019 (Figure 1). The time series is presented from 2015 onwards since
338 enough data is accumulated at this point to obtain a synoptical view that represents all
339 basins and environmental zones defined within the Southern Ocean. In order to reduce the
340 noise in the temporal signal and obtain a clear seasonal pattern of the blooms, we first
341 smooth the Southern Ocean time series by applying a moving average filter over a 10 days
342 window. Subsequently, we applied a secondary moving filter over 500 consecutive data points
343 to reduce small temporal variability that propagates into the computation of the temporal
344 derivatives. The mean annual cycle of r, μ, dμ/dt, and dMLD/dt for each of the environ-
345 mental zones (STZ, SAZ, PAZ, and SIZ, Figures 2 and 3) is obtained by averaging all weekly
346 data available within each zone, in order to create a weekly-resolved annual climatology of
347 all float data (spanning between 2012 and 2019). The annual climatology is subsequently
348 smoothed applying a moving average filter over a 60 days window.

16

Environmental zones

Environmental zones defined in the Southern Ocean[48] are based on a mean 2004–2014 Argo-based climatology of temperature and salinity[49] (Figure S1). The Subtropical Zone (STZ), which roughly covers the oligotrophic oceanic section between 30°S and 40°S, is characterized by reduced surface nutrient concentrations and constrained to the south by the Subtropical Front. The Subantarctic Zone (SAZ) and Polar Antarctic Zone (PAZ), which cover the circumpolar section of the Southern Ocean approximately constrained between 40°S and 60°S, are characterized by deep mixed layers, high vertical mixing, elevated macronutrient concentrations (i.e., nitrate, phosphate, silicate), and growth-limiting surface iron concentrations[27,28,21]. The Seasonal Ice Zone (SIZ), which represents the seasonally ice-covered zone of the Southern Ocean, extends between Antarctica and approximately 60°S. Biogeochemical properties in the surface mixed layer sampled by the floats show clear latitudinal gradients across zones summarized in[50]: Temperature decreases from $> 15°C$ in the STZ to $\sim 10°C$ in the SAZ and $< 5°C$ towards the SIZ. Mean oxygen in the mixed layer increases from $<$ 250 μmol O$_2$ kg^{-1} in the STZ to $\sim$ 270 μmol O$_2$ kg^{-1} in the SAZ, and > 300 μmol O$_2$ kg^{-1} south of the antarctic polar front. Nitrate also shows a meridional increase from < 5 μmol NO$_3$ kg^{-1} in the STZ to > 10 μmol NO$_3$ kg^{-1} in the SAZ, and > 20 μmol NO$_3$ kg^{-1} south of the polar front, towards the SIZ (Figure S1).

Modeling changes in phytoplankton bloom cycles and magnitude

The present mean phytoplankton biomass annual cycle in the Southern Ocean is computed by averaging all float-based estimates of mean phytoplankton carbon concentration in the mixed layer on a weekly basis and interpolating them into a daily time series (Figure 4a). The same procedure is followed to obtain an annual climatology of r and μ. Seasonal anomalies in μ are calculated by subtracting the climatological daily value of μ from the overall annual mean of μ. Relative changes in μ are computed by decreasing daily μ when

17

the seasonal anomaly is positive (larger than the annual mean), and increasing it when the seasonal anomaly is negative (lower than the annual mean) (Figure S7a). The rationale for this sensitivity exercise is that future increases in ocean stratification should increase nutrient limitation during summer (period of positive anomalies) and relax light limitation during winter (period of negative anomalies). The division rate (μ) is decreased/increased over a range from 10% to 60% with respect to current values during winter and summer, respectively. The accumulation rate (r) for each scenario was calculated following Equation 1: $r = \mu - l$. The climatological loss rate (l) for each scenario (between 10 and 60 %) is obtained as a 2-days temporally lagged μ. The 2-days lag was determined by reconstructing present accumulation rates as $r = \mu - \mu_{xday-lag}$[10], over a range of temporal lags in $\mu_{xday-lag}$ between 1 and 10 days. The best reconstruction of present r was obtained with a temporal lag of 2 days in μ (Figure S6). Finally, the climatological phytoplankton concentration for each scenario is obtained from a numerical integration of the modeled r using the first value of the current climatological annual cycle as the initial boundary condition (i.e., phytoplankton carbon concentration corresponding to the first day of January). Annual cycles of vertically integrated net primary production are obtained as the product of climatological division rates (μ) and integrated phytoplankton carbon inventories obtained for each variation of μ (i.e., between 10 and 60 %) (Figure S7b).

Acknowledgments
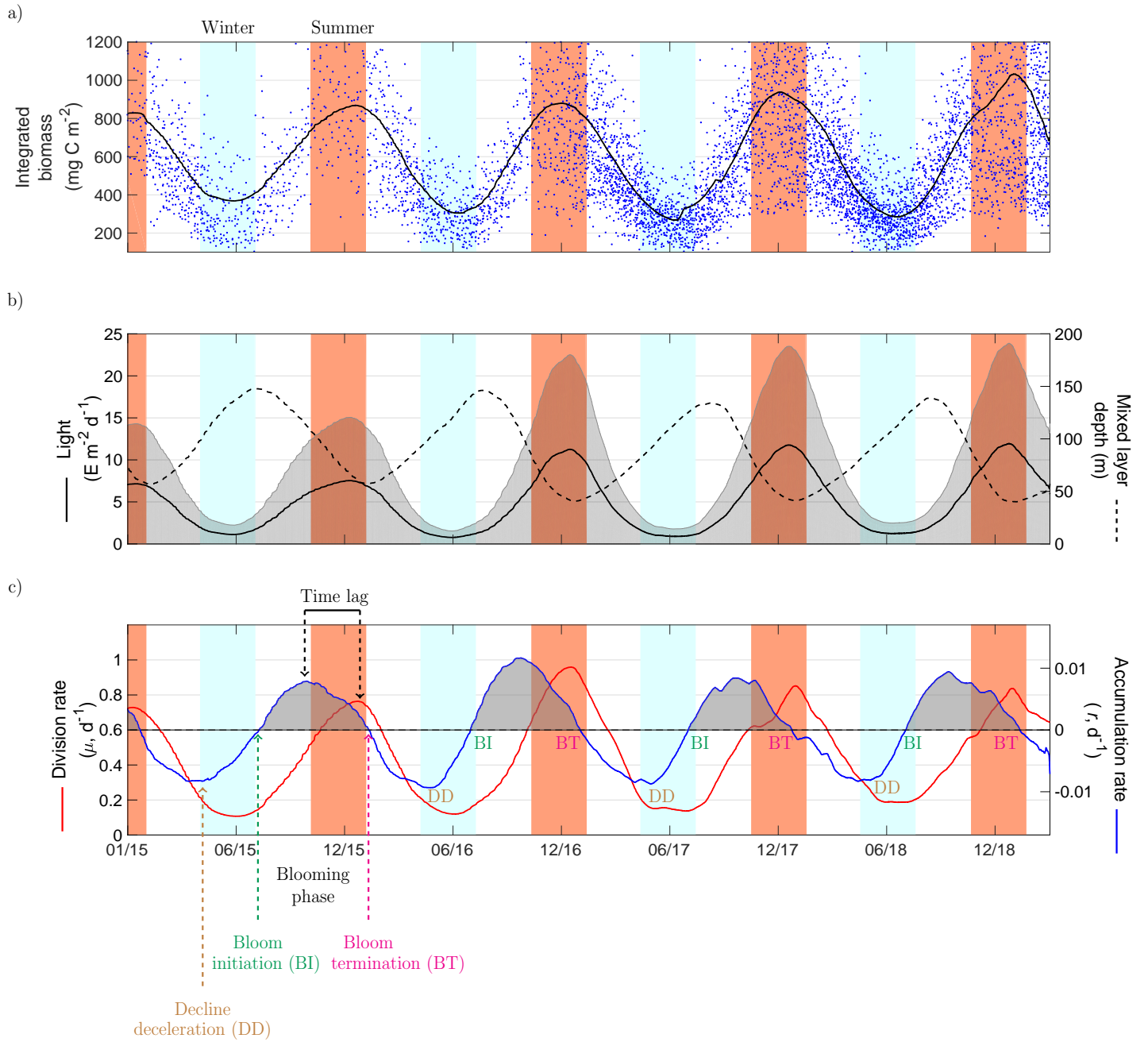
Figure 1: **Annual cycles of phytoplankton biomass in the Southern Ocean.** (a) Annual cycles of phytoplankton carbon integrated from surface to the depth of the mixed layer or euphotic depth (whichever is deeper). Blue dots: Individual float observations. Continuous black line: Average time series from individual observations. (b) Black continuous line: Average time series of the mean light level in the surface mixed layer in the Southern Ocean computed as photosynthetically active radiation (PAR) (shaded area represents the standard deviation). Black dashed line: Average time series of the depth of the surface mixed layer. (c) Red continuous line: Average time series of phytoplankton division rates (μ). Blue continuous line: Average time series of phytoplankton net accumulation rate (r). The phytoplankton blooming phase is defined as the time period where $r > 0$, constrained between the time of 'Bloom initiation' (BI) and 'Bloom termination' (BT) of each annual cycle. The 'Decline deceleration' (DD) point, indicates the moment where the autumn decline in biomass starts to decelerate prior to the onset of the bloom. Seasonally, a clear 'Time lag' exist between μ and r where highest accumulation rates are observed approximately 3 months before the peak in division rates. Light blue and red shaded panels indicate austral winter (May-August) and summer (November-February) months, respectively. See Methods for details on the smoothing of time series.
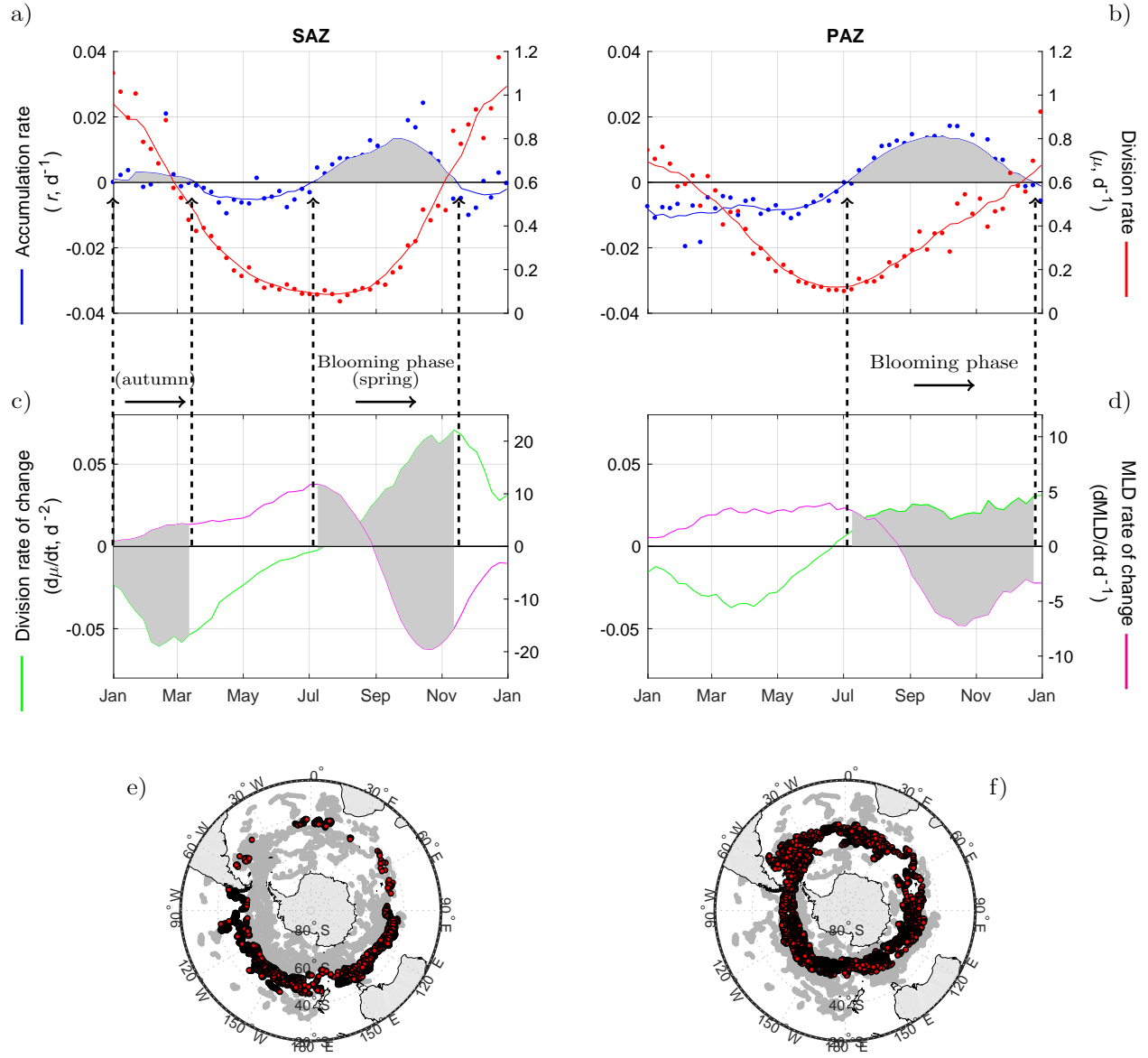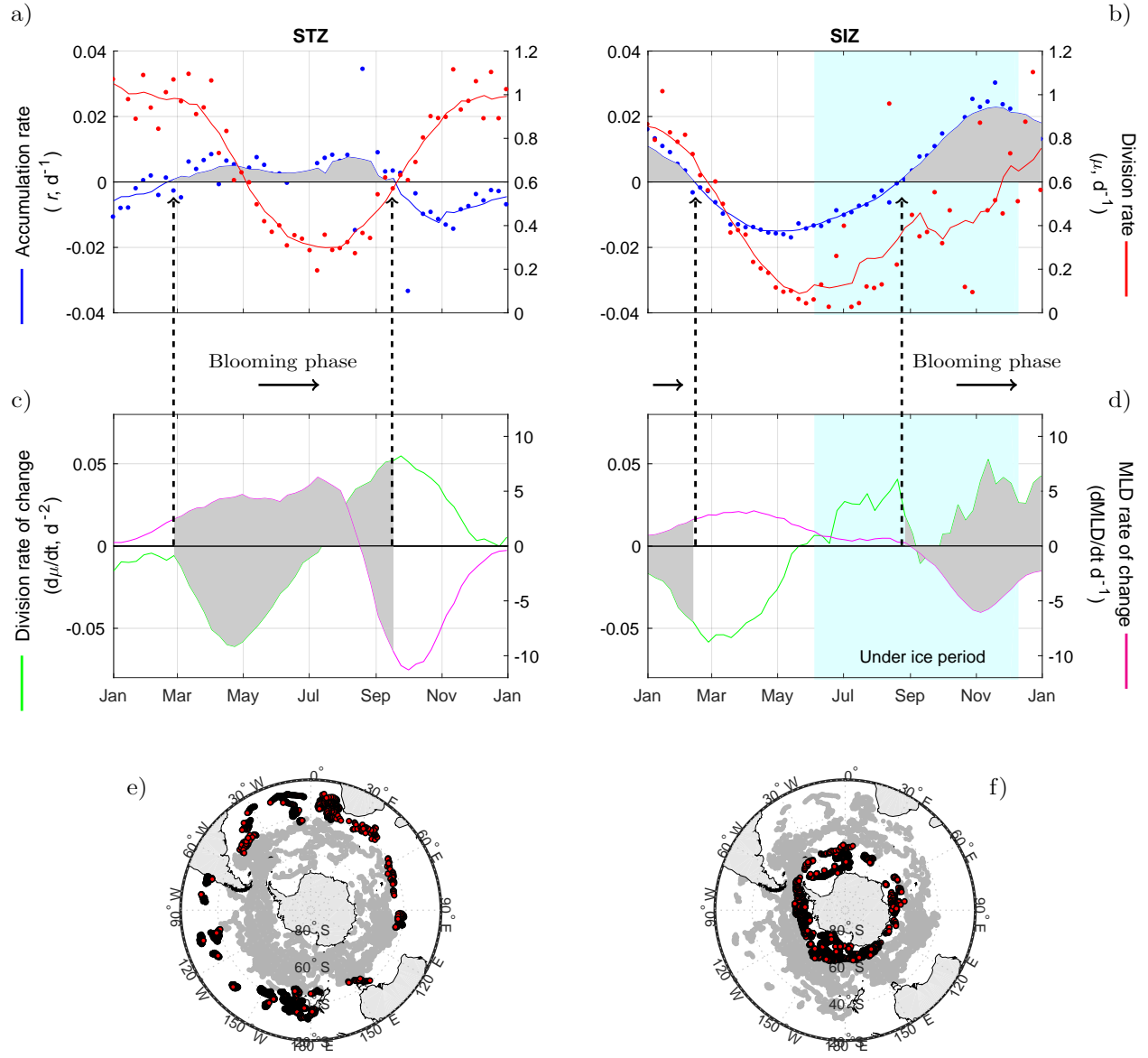
Figure 2: **Climatological bloom cycles in the the Subantarctic and Polar Antarctic Zone (SAZ and PAZ).** (a and b) Annual cycle of phytoplankton accumulation (r, blue line) and division rates (μ, red lines) for the SAZ and PAZ. Individual points are weekly averaged observations and continuous line is the result of a smoothing temporal filter (Methods). (c and d) Averaged time series of the temporal derivative of μ (dμ/dt, green line) and of the mixed layer depth (MLD) (dMLD/dt, magenta line). The blooming phase ($r > 0$) is highlighted by the gray shaded periods. (e and f) Bottom maps: Location of float profiles deployed in the SAZ and PAZ.

Figure 3: **Climatological bloom cycles in the the Subtropical and Seasonal Ice Zone (STZ and SIZ).** (a and b) Annual cycle of phytoplankton accumulation (r, blue line) and division rates (μ, red lines) for the STZ and SIZ. Individual points are weekly averaged observations and continuous line is the result of a smoothing temporal filter (Methods). (c and d) Averaged time series of the temporal derivative of μ (dμ/dt, green line) and of the mixed layer depth (MLD) (dMLD/dt, magenta line). The blooming phase ($r > 0$) is highlighted by the gray shaded periods. Light blue shaded section indicates the period where 50 % or more profiles where under ice. (e and f) Bottom maps: Location of float profiles deployed in the STZ and SIZ.

21
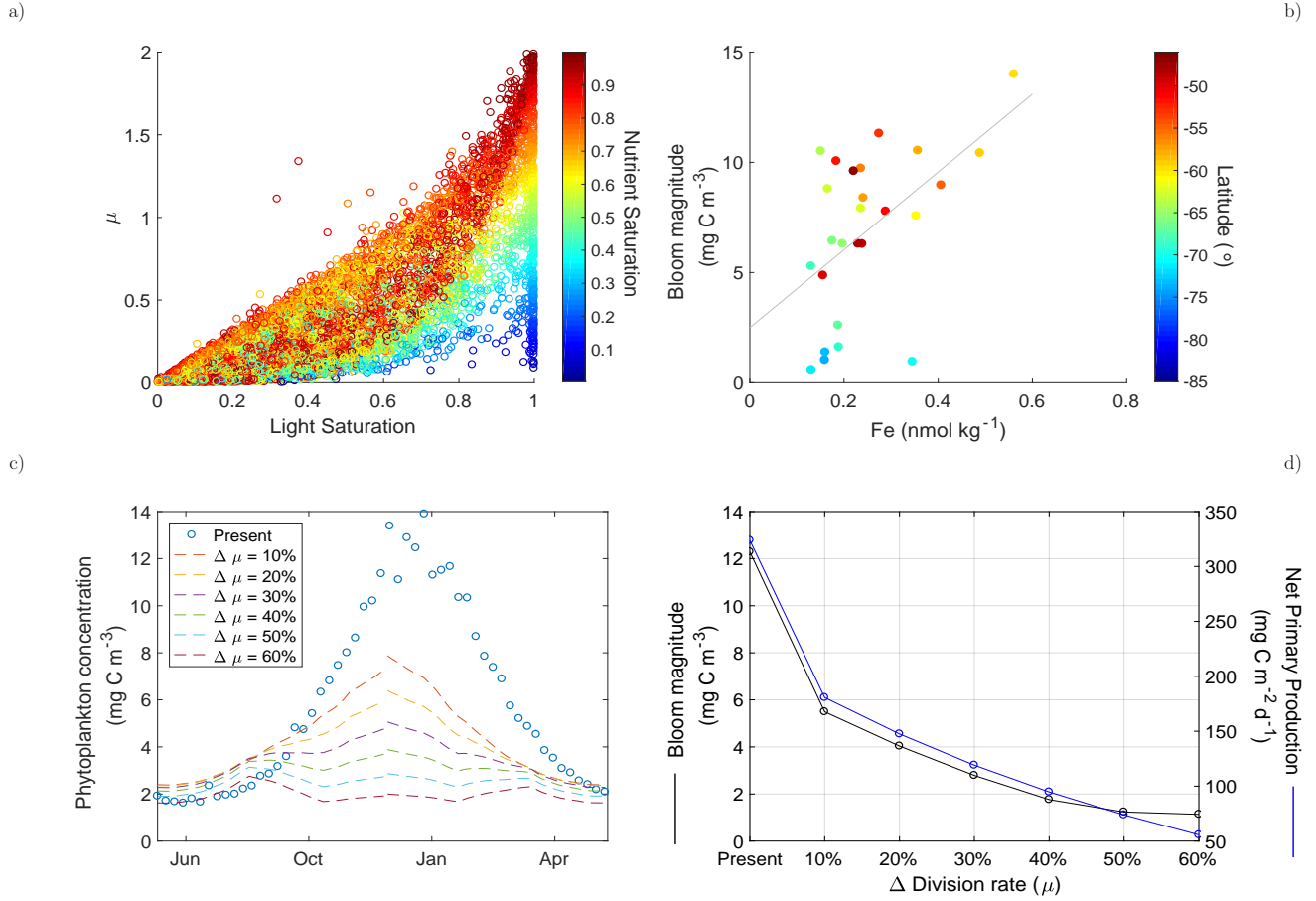
Figure 4: **Light and iron controls on phytoplankton blooms and future projections of biomass and productivity.** (a) Relationship between the phytoplankton division rate (μ) and the light and nutrient saturation index diagnosed by the phytoplankton growth model. (b) Relationship between bloom magnitude and the surface iron concentration in the Southern Ocean. Continuous black line is obtained from a least-squares linear regression model with a coefficient of determination (R^2) of 0.26 and a p-value < 0.05. (c) Variations in seasonal phytoplankton concentration in the Southern Ocean resulting from a relative decrease (increase) in μ during summer (winter) with respect to the present division rate. (d) Decrease in mean phytoplankton bloom magnitude (BM, black line and symbols) and annual mean vertically integrated net primary production (NPP, blue line and symbols) in the Southern Ocean as a consequence of relative changes in μ.

References

1. Parekh, P., Dutkiewicz, S., Follows, M. J. & Ito, T. Atmospheric carbon dioxide in a less dusty world. *Geophysical Research Letters* **33** (2006). URL `https://agupubs.onlinelibrary.wiley.com/doi/abs/10.1029/2005GL025098`. `https://agupubs.onlinelibrary.wiley.com/doi/pdf/10.1029/2005GL025098`.

2. Longhurst, A. R. Biogeographic partition of the ocean. In Longhurst, A. R. (ed.) *Ecological Geography of the Sea (Second Edition)*, 19 – 34 (Academic Press, Burlington, 2007), second edition edn. URL `http://www.sciencedirect.com/science/article/pii/B9780124555211500036`.

3. Sverdrup, H. U. On conditions for the vernal blooming of phytoplankton. *Journal du Conseil International pour l' Exploration de la Mer.* **18**, 287–295 (1953).

4. Gran, H. H. & Braarud, T. A Quantitative Study of the Phytoplankton in the Bay of Fundy and the Gulf of Maine (including Observations on Hydrography, Chemistry and Turbidity). *Journal of the Biological Board of Canada* **1**, 279–467 (1935). URL `https://doi.org/10.1139/f35-012`. `https://doi.org/10.1139/f35-012`.

5. Gran, H. H. Phytoplankton. methods and problems. *Journal du Conseil International Pour l'Exoploration de la Mer* **7**, 343–358 (1932).

6. Atkins, W. R. G. The chemistry of sea-water in relation to the productivity of the sea. *Science Progress* **7**, 298–312 (1932).

7. Uchida, T. *et al.* Southern ocean phytoplankton blooms observed by biogeochemical floats. *Journal of Geophysical Research: Oceans* (2019). URL `https://agupubs.onlinelibrary.wiley.com/doi/abs/10.1029/2019JC015355`. `https://agupubs.onlinelibrary.wiley.com/doi/pdf/10.1029/2019JC015355`.

8. Banse, K. Grazing, Temporal Changes of Phytoplankton Concentrations, and the Microbial Loop in the Open Sea. In Falkowski, P. G., Woodhead, A. & Vivirito, K. (eds.) *Primary Productivity and Biogeochemical Cycles in the Sea*, vol. 43 of *Environmental Science Research*, 409 – 440 (Springer US, Boston, MA, 1992). URL https://link.springer.com/chapter/10.1007/978-1-4899-0762-2_22.

9. Evans, G. T. & Parslow, J. S. A model of annual plankton cycles. *Biological Oceanography* **3**, 327–347 (1985).

10. Behrenfeld, M. J. & Boss, E. S. Student's tutorial on bloom hypotheses in the context of phytoplankton annual cycles. *Global Change Biology* **24**, 55–77 (2018). URL https://onlinelibrary.wiley.com/doi/abs/10.1111/gcb.13858. https://onlinelibrary.wiley.com/doi/pdf/10.1111/gcb.13858.

11. Behrenfeld, M. J. Abandoning Sverdrup's critical depth hypothesis on phytoplankton blooms. *Ecology* **91**, 977–989 (2010).

12. Boss, E. & Behrenfeld, M. In situ evaluation of the initiation of the North Atlantic phytoplankton bloom. *Geophysical Research Letters* **37** (2010). URL http://dx.doi.org/10.1029/2010GL044174. L18603.

13. Mignot, A., Ferrari, R. & Claustre, H. Floats with bio-optical sensors reveal what processes trigger the North Atlantic bloom. *Nature Communications* **9**, 190 (2018). URL https://doi.org/10.1038/s41467-017-02143-6.

14. Westberry, T. K. *et al.* Annual cycles of phytoplankton biomass in the subarctic atlantic and pacific ocean. *Global Biogeochemical Cycles* **30**, 175–190 (2016). URL https://agupubs.onlinelibrary.wiley.com/doi/abs/10.1002/2015GB005276. https://agupubs.onlinelibrary.wiley.com/doi/pdf/10.1002/2015GB005276.

15. Behrenfeld, M. J. *et al.* Annual boom-bust cycles of polar phytoplankton biomass revealed by space-based lidar. *Nature Geoscience* **10**, 118–122 (2017). URL `http://dx.doi.org/10.1038/ngeo2861`.

16. Behrenfeld, M. J. Climate-mediated dance of the plankton. *Nature Climate Change* **4**, 880–887 (2014). URL `https://doi.org/10.1038/nclimate2349`.

17. Banse, K. Grazing and zooplankton production as key controls of phytoplankton production in the open ocean. *Oceanography* **7**, 13 – 20 (1994). URL `https://doi.org/10.5670/oceanog.1994.10`.

18. Behrenfeld, M. J. & Milligan, A. J. Photophysiological expressions of iron stress in phytoplankton. *Annual Review of Marine Science* **5**, 217–246 (2013). URL `https://doi.org/10.1146/annurev-marine-121211-172356`. PMID: 22881354, `https://doi.org/10.1146/annurev-marine-121211-172356`.

19. Behrenfeld, M. J., Doney, S. C., Lima, I., Boss, E. S. & Siegel, D. A. Annual cycles of ecological disturbance and recovery underlying the subarctic atlantic spring plankton bloom. *Global Biogeochemical Cycles* **27**, 526–540 (2013). URL `https://agupubs.onlinelibrary.wiley.com/doi/abs/10.1002/gbc.20050`. `https://agupubs.onlinelibrary.wiley.com/doi/pdf/10.1002/gbc.20050`.

20. Zehr, J. P. & Ward, B. B. Nitrogen cycling in the ocean: New perspectives on processes and paradigms. *Applied and Environmental Microbiology* **68**, 1015–1024 (2002). URL `https://aem.asm.org/content/68/3/1015`. `https://aem.asm.org/content/68/3/1015.full.pdf`.

21. Moore, C. M. *et al.* Processes and patterns of oceanic nutrient limitation. *Nature Geoscience* **6** (2013). URL `http://www.nature.com/doifinder/10.1038/ngeo1765`.

466   22. Wong, A. P. S. & Riser, S. C. Profiling float observations of the upper ocean under sea

467   ice off the wilkes land coast of antarctica. *Journal of Physical Oceanography* **41**, 1102–

468   1115 (2011). URL `https://doi.org/10.1175/2011JPO4516.1`. `https://doi.org/10.`

469   `1175/2011JPO4516.1`.

470   23. Johnson, K. S. *et al.* Biogeochemical sensor performance in the SOCCOM profiling float

471   array. *Journal of Geophysical Research: Oceans* **122**, 6416–6436 (2017).

472   24. Arrigo, K. R. *et al.* Massive phytoplankton blooms under arctic sea ice. *Science* **336**,

473   1408–1408 (2012). URL `https://science.sciencemag.org/content/336/6087/1408`.

474   `https://science.sciencemag.org/content/336/6087/1408.full.pdf`.

475   25. Arrigo, K. R. *et al.* Early spring phytoplankton dynamics in the western antarctic penin-

476   sula. *Journal of Geophysical Research: Oceans* **122**, 9350–9369 (2017). URL `https:`

477   `//agupubs.onlinelibrary.wiley.com/doi/abs/10.1002/2017JC013281`. `https://`

478   `agupubs.onlinelibrary.wiley.com/doi/pdf/10.1002/2017JC013281`.

479   26. Geider, R. J., Platt, T. & Raven, J. Size dependence of growth and photosynthesis

480   in diatoms: a synthesis. *Marine Ecology. Progress Series* **30**, 93–104 (1986). URL

481   `http://www.int-res.com/articles/meps/30/m030p093.pdf`.

482   27. Martin, J., Gordon, R. M. & Fitzwater, S. E. Iron in Antartic waters. *Nature* **345**,

483   156–158 (1990). Doi:10.1038/345156a0.

484   28. Boyd, P. W. *et al.* Mesoscale iron enrichment experiments 1993-2005: Synthesis and

485   future directions. *Science* **315**, 612–617 (2007). URL `http://www.ncbi.nlm.nih.gov/`

486   `pubmed/17272712`.

487   29. Sarmiento, J. L. *et al.* Response of ocean ecosystems to climate warming. *Global Bio-*

488   *geochemical Cycles* **18**, GB3003 (2004). Doi:10.1029/2003GB002134.

30. Riebesell, U., Körtzinger, A. & Oschlies, A. Sensitivities of marine carbon fluxes to ocean change. *Proceedings of the National Academy of Sciences* **106**, 20602–20609 (2009). URL `http://www.pnas.org/content/106/49/20602.abstract`. `http://www.pnas.org/content/106/49/20602.full.pdf+html`.

31. Gruber, N. *et al.* Oceanic sources, sinks, and transport of atmospheric CO_2. *Global Biogeochemical Cycles* **23** (2009). URL `https://agupubs.onlinelibrary.wiley.com/doi/abs/10.1029/2008GB003349`. `https://agupubs.onlinelibrary.wiley.com/doi/pdf/10.1029/2008GB003349`.

32. Gruber, N., Landschtzer, P. & Lovenduski, N. S. The variable Southern Ocean carbon sink. *Annual Review of Marine Science* **11**, 159–186 (2019). URL `https://doi.org/10.1146/annurev-marine-121916-063407`. PMID: 30212259, `https://doi.org/10.1146/annurev-marine-121916-063407`.

33. Sarmiento, J. L., Gruber, N., Brzezinski, M. A. & Dunne, J. P. High-latitude controls of thermocline nutrients and low latitude biological productivity. *Nature* **427**, 56–60 (2004).

34. Pahlow, M. & Prowe, F. Model of optimal current feeding in zooplankton. *Marine Ecology Progress Series* **403**, 129–144 (2010).

35. Johnson, K. S. *et al.* SOCCOM float data — Snapshot 2019-03-12. In *Southern Ocean Carbon and Climate Observations and Modeling (SOCCOM) Float Data Archive* (UC San Diego Library Digital Collections, 2019).

36. Haëntjens, N., Boss, E. & Talley, L. D. Revisiting ocean color algorithms for chlorophyll a and particulate organic carbon in the Southern Ocean using biogeochemical floats. *Journal of Geophysical Research: Oceans* (2017). URL `http://dx.doi.org/10.1002/2017JC012844`.

27

37. Graff, J. R. *et al.* Analytical phytoplankton carbon measurements spanning diverse ecosystems. *Deep Sea Research Part I: Oceanographic Research Papers* **102**, 16 – 25 (2015). URL `http://www.sciencedirect.com/science/article/pii/S0967063715000801`.

38. Behrenfeld, M. J., Doney, S. C., Lima, I., Boss, E. S. & Siegel, D. A. Reply to a comment by stephen m. chiswell on: annual cycles of ecological disturbance and recovery underlying the subarctic atlantic spring plankton bloom by m. j. behrenfeld et al. (2013). *Global Biogeochemical Cycles* **27**, 1294–1296 (2013). URL `https://agupubs.onlinelibrary.wiley.com/doi/abs/10.1002/2013GB004720`. `https://agupubs.onlinelibrary.wiley.com/doi/pdf/10.1002/2013GB004720`.

39. de Boyer Montégut, C., Madec, G., Fischer, A. S., Lazar, A. & Iudicone, D. Mixed layer depth over the global ocean: An examination of profile data and a profile-based climatology. *Journal of Geophysical Research: Oceans* **109** (2004). URL `http://dx.doi.org/10.1029/2004JC002378`. C12003.

40. Tagliabue, A. *et al.* A global compilation of dissolved iron measurements: focus on distributions and processes in the southern ocean. *Biogeosciences* **9**, 2333–2349 (2012). URL `https://www.biogeosciences.net/9/2333/2012/`.

41. Westberry, T., Behrenfeld, M. J., Siegel, D. A. & Boss, E. Carbon-based primary productivity modeling with vertically resolved photoacclimation. *Global Biogeochemical Cycles* **22**, GB2024 (2008).

42. Ricchiazzi, P., Yang, S., Gautier, C. & Sowle, D. SBDART: A Research and Teaching Software Tool for Plane-Parallel Radiative Transfer in the Earth's Atmosphere. *Bulletin of the American Meteorological Society* **79**, 2101–2114 (1998). URL `https://doi.org/10.1175/1520-0477(1998)079<2101:SARATS>2.0.CO;2`.

43. Banse, K. Rates of phytoplankton cell division in the field and in iron enrichment experiments. *Limnology and Oceanography* **36**, 1886–1898 (1991). URL https://aslopubs.onlinelibrary.wiley.com/doi/abs/10.4319/lo.1991.36. 8.1886. https://aslopubs.onlinelibrary.wiley.com/doi/pdf/10.4319/lo.1991. 36.8.1886.

44. Behrenfeld, M. J., Boss, E., Siegel, D. A. & Shea, D. M. Carbon-based ocean productivity and phytoplankton physiology from space. *Global Biogeochemical Cycles* **19**, GB1006 (2005). Doi:10.1029/2004GB002299.

45. Geider, R. J. Light and temperature dependence of the carbon to chorophyll ratio in microalgae an cyanobacteria:Implications for physiology and growth of phytoplankton. *New Phytologist* **106**, 1–34 (1987). URL http://dx.doi.org/10.1111/j.1469-8137. 1987.tb04788.x.

46. Arteaga, L., Pahlow, M. & Oschlies, A. Global patterns of phytoplankton nutrient and light colimitation inferred from an optimality-based model. *Global Biogeochemical Cycles* **28**, 648–661 (2014). URL http://dx.doi.org/10.1002/2013GB004668.

47. Geider, R. J. & LaRoche, J. The role of iron in phytoplankton photosynthesis, and the potential for iron-limitation of primary productivity in the sea. *Photosynthesis Research* **39**, 275–301 (1994).

48. Orsi, A. H., Whitworth, T. & Nowlin, W. D. On the meridional extent and fronts of the Antarctic Circumpolar Current. *Deep Sea Research Part I: Oceanographic Research Papers* **42**, 641 – 673 (1995). URL http://www.sciencedirect.com/science/article/ pii/096706379500021W.

49. Roemmich, D. & Gilson, J. The 2004–2008 mean and annual cycle of temperature, salinity, and steric height in the global ocean from the argo program. *Progress in Oceanog-*

561   *raphy* **82**, 81 – 100 (2009). URL `http://www.sciencedirect.com/science/article/`

562   `pii/S0079661109000160`.

563 50. Arteaga, L. A., Pahlow, M., Bushinsky, S. M. & Sarmiento, J. L. Nutri-

564   ent Controls on Export Production in the Southern Ocean. *Global Biogeochem-*

565   *ical Cycles* (2019). URL `https://agupubs.onlinelibrary.wiley.com/doi/abs/`

566   `10.1029/2019GB006236`. `https://agupubs.onlinelibrary.wiley.com/doi/pdf/10.`

567   `1029/2019GB006236`.

Supplementary information for

Ecological drivers of phytoplankton bloom cycles in the Southern Ocean

Lionel A. Arteaga[1*], Emmanuel Boss [2], Michael J. Behrenfeld [3], Toby Westberry [3], Jorge L. Sarmiento [1]

(*) Corresponding author

Afiliations:

- (1) Program in Atmospheric and Oceanic Sciences, Princeton University, 300 Forrestal Rd, Princeton, NJ, USA,

- (2) School of Marine Sciences, 5706 Aubert Hall, University of Maine, Orono, Maine 04469−5741, USA.

- (3) Department of Botany and Plant Pathology, Cordley Hall 2082, Oregon State University, Corvallis, Oregon 97331−2902, USA.

For the present study, BGC-Argo float data deployed by the SOCCOM program between 2012 and 2019 was analyzed altogether and subdivided into environmental zone as explained in the Methods section. The Southern Ocean presents a clear spatial gradient in surface mixed layer biogeochemical properties (temperature, oxygen, and nitrate) across the four environmental zones defined in this study (Figure S1). Annual climatologies of float-sampled mean mixed layer nitrate, up-to-date compiled dissolved iron observations[1] (Figure S2), and satellite based mixed layer light estimates (Figure S3) were produced and analyzed for each environmental zone in conjunction with temporal changes in phytoplankton biomass.

Individual float-based estimates of phytoplankton division rates (μ) and net accumulation rates based on changes in mixed layer biomass concentration (r_{mld}) and integrated inventory (r_{int}) were obtained as detailed in the Methods section (Figure S4). The seasonality of r_{mld}

is similar to that of r_{int}. However, clear differences exist during periods of mixed layer shoaling or deepening. Net accumulation rates based on the mixed layer integrated inventory of biomass (r_{int}) are higher than rates based on changes in the biomass concentration (r_{mld}) during periods of mixed layer deepening, and vice versa (Figure S5). This pattern is consistent with the expected effect of dilution of the mixed layer phytoplankton concentration during increased surface vertical mixing on the computation of accumulation rates based on biomass concentration, and the expected effect from changes in the vertically integrated water layer on the computation of biomass accumulation based on the integrated phytoplankton carbon inventory in the seasonally varying mixed layer[2,3]. The smoothed time series of r_{int} - r_{mld} and the temporal derivative of the mixed layer (dMLD/dt) are computed as described in the Methods section.

The analysis of future changes in phytoplankton bloom magnitude and net primary production is based on the reconstruction of the climatological phytoplankton loss rate for the Southern Ocean based on a 2-days temporal lag in μ[4] (Figure S6). The reconstruction of the mean loss rate (l) in the Southern Ocean permitted the assessment of the sensitivity of vertically integrated net primary productivity to induced changes in the climatological seasonal cycle of phytoplankton division rate (μ) (Figure S7).
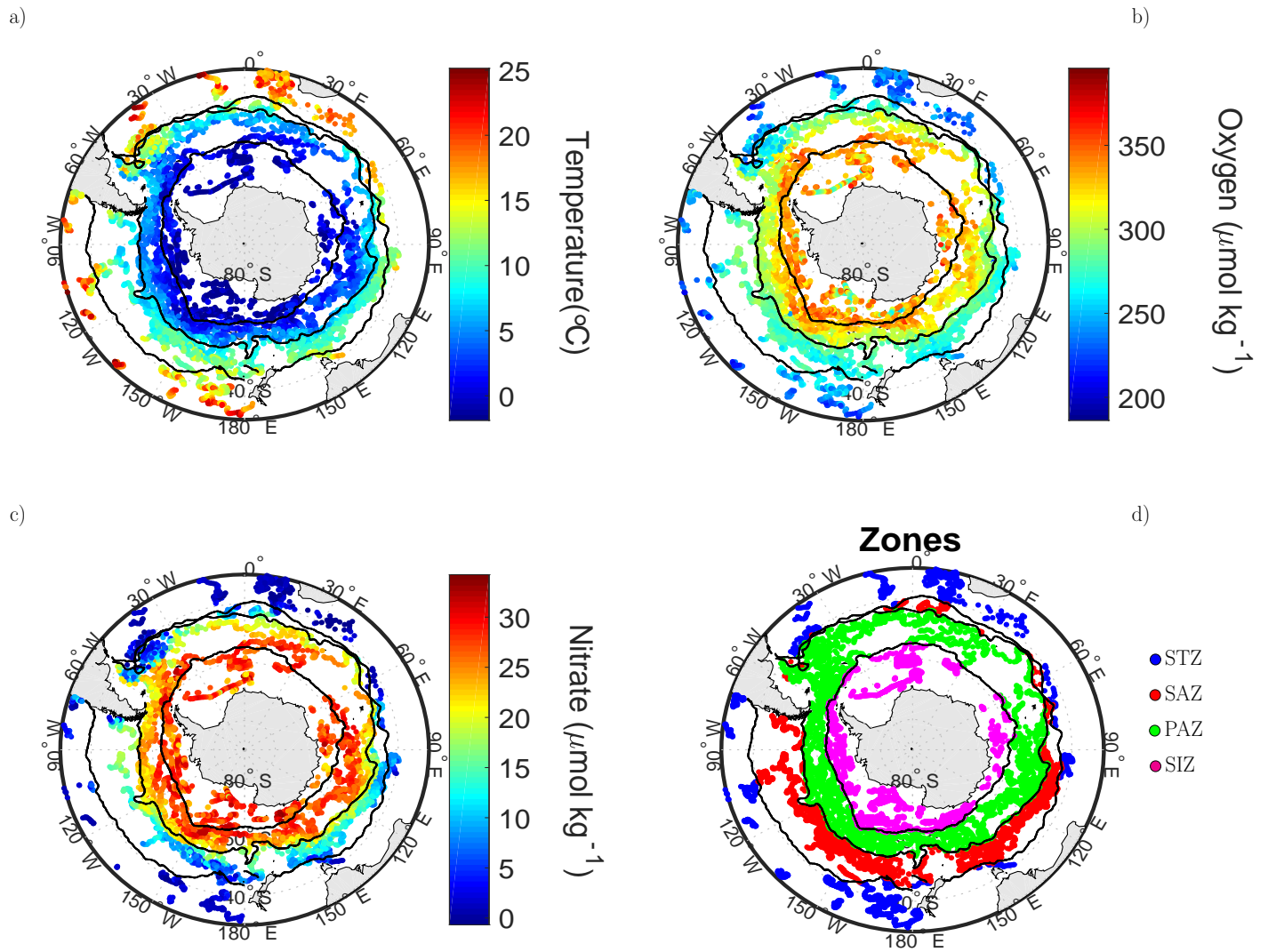
Figure S1: Gradients in mean surface mixed layer (a) temperature, (b) dissolved oxygen, and (c) nitrate concentration measured by the biogeochemical floats. (d) Location of the Southern Ocean environmental zones defined in this study: Subtropical Zone (STZ), Subantarctic Zone (SAZ), Polar Antarctic Zone (PAZ), and Seasonal Ice Zone (SIZ).
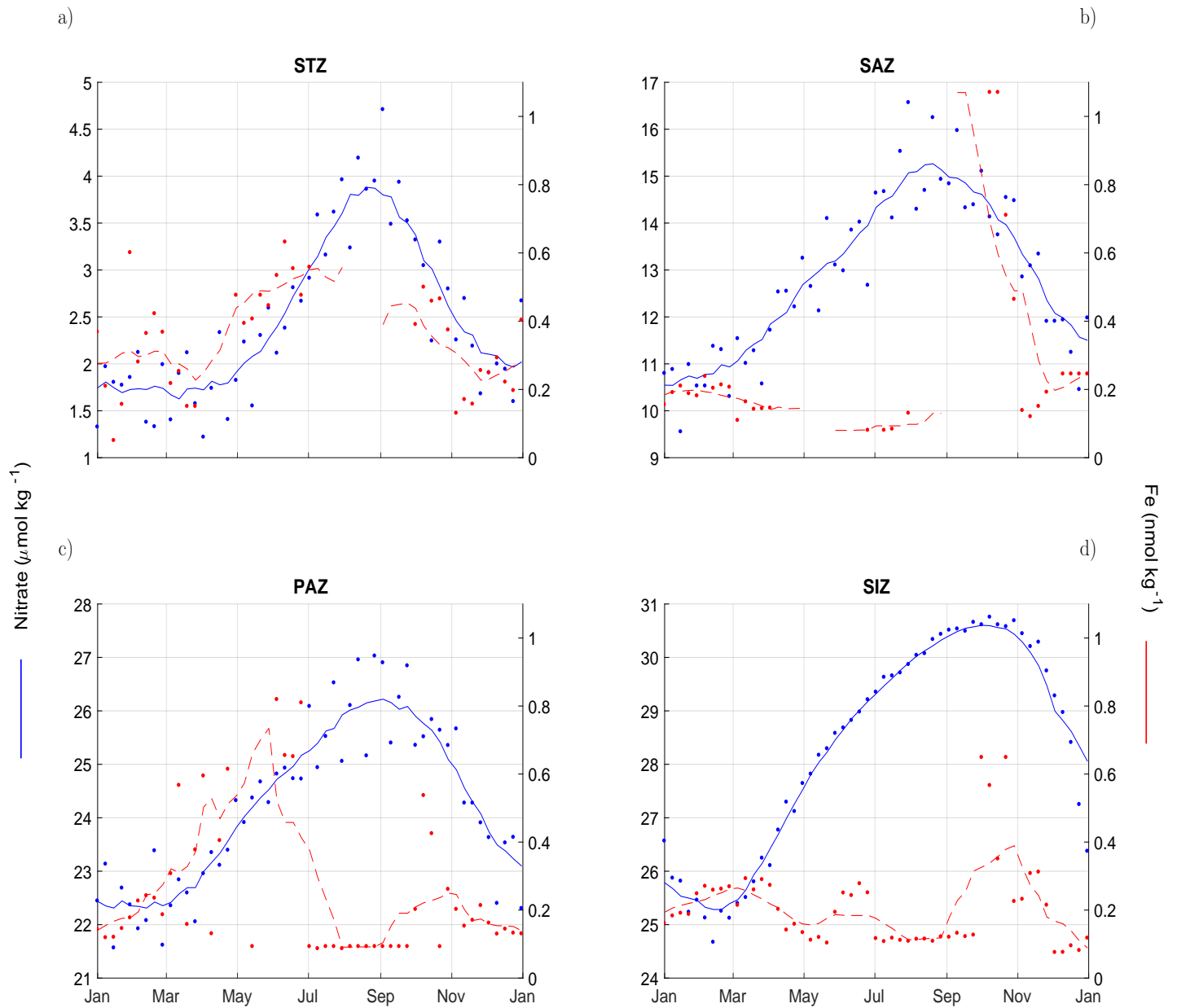
a)

b)

c)

d)

Figure S2: Annual climatology of nitrate and and dissolved iron (Fe) concentration in the surface mixed layer for each environmental zone defined in the Southern Ocean: (a) STZ, (b) SAZ, (c) PAZ, and (d) SIZ. Individual points are weekly averaged observations and continuous line is the result of a smoothing temporal filter over a 60 days window.
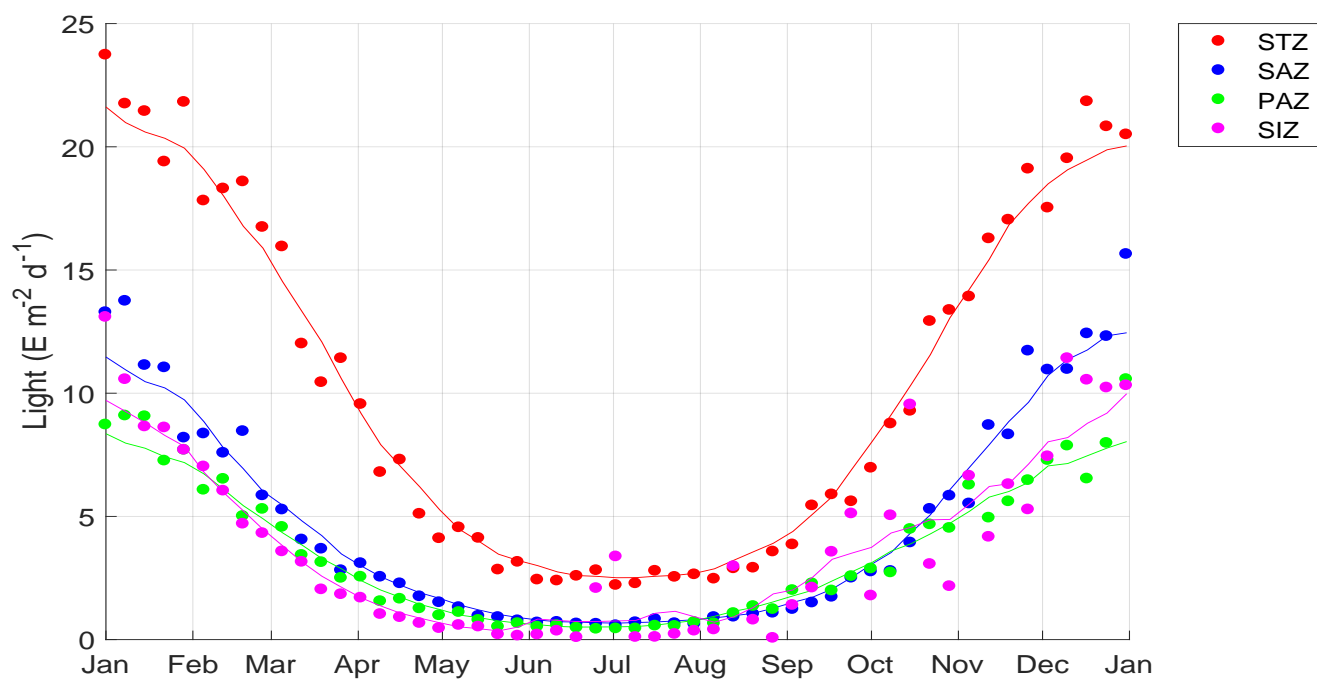
Figure S3: Annual climatology of mean mixed layer light for each environmental zone defined in the Southern Ocean. Individual points are weekly averaged observations and continuous line is the result of a smoothing temporal filter over a 60 days window.
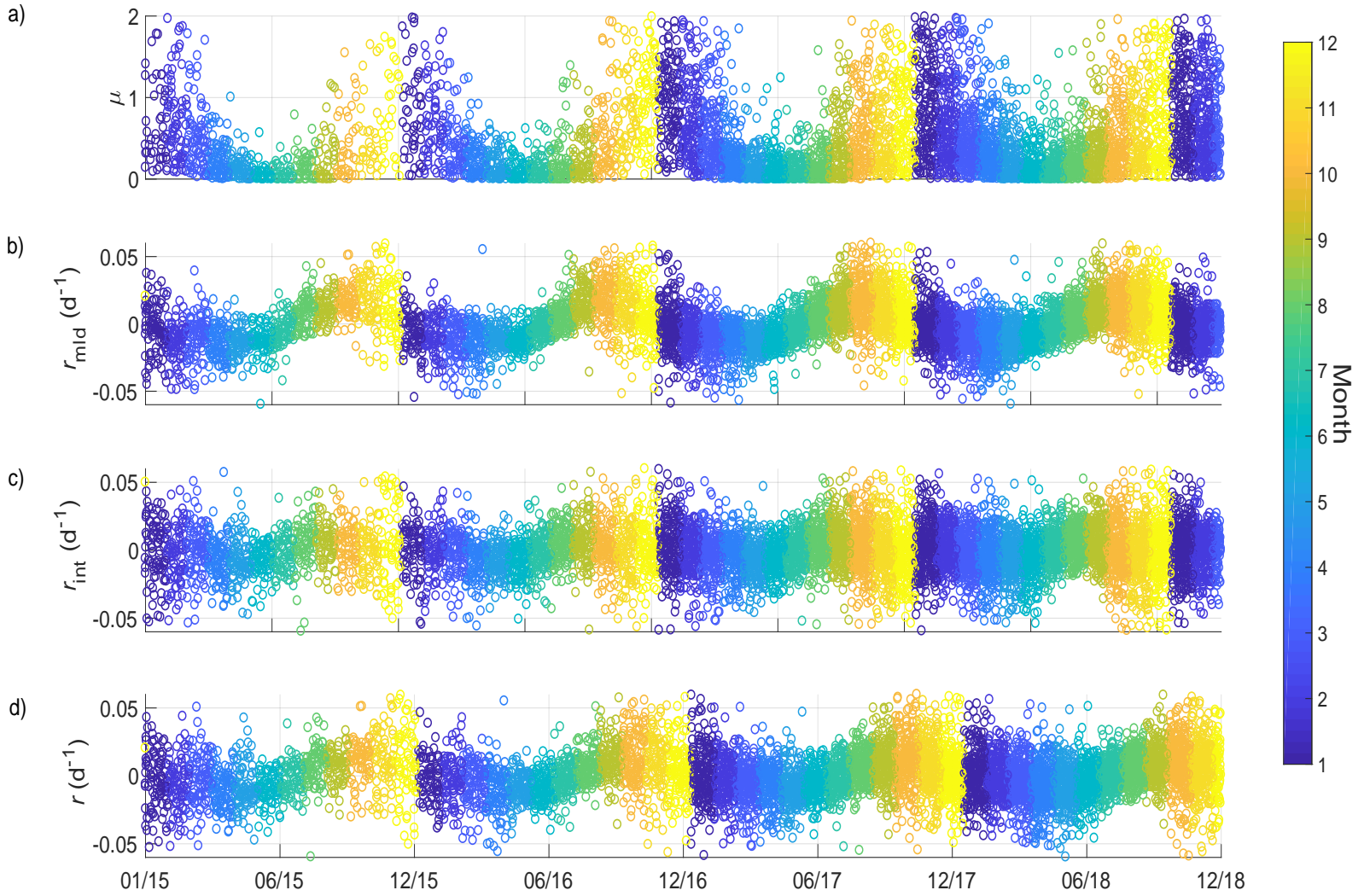
Figure S4: (a) Individual float-based estimates of phytoplankton division rate (μ) from the growth of model employed in this study[5], averaged in the mixed layer. (b) Individual float-based estimates of r based on changes in mixed layer phytoplankton biomass concentration (r_{mld}) and (c) based on the integrated biomass inventory (r_{int}). (d) Final estimate of net accumulation rate (r) based on the switching algorithm (Equation 4). Colorbar indicates the month of each observationally-based estimate.
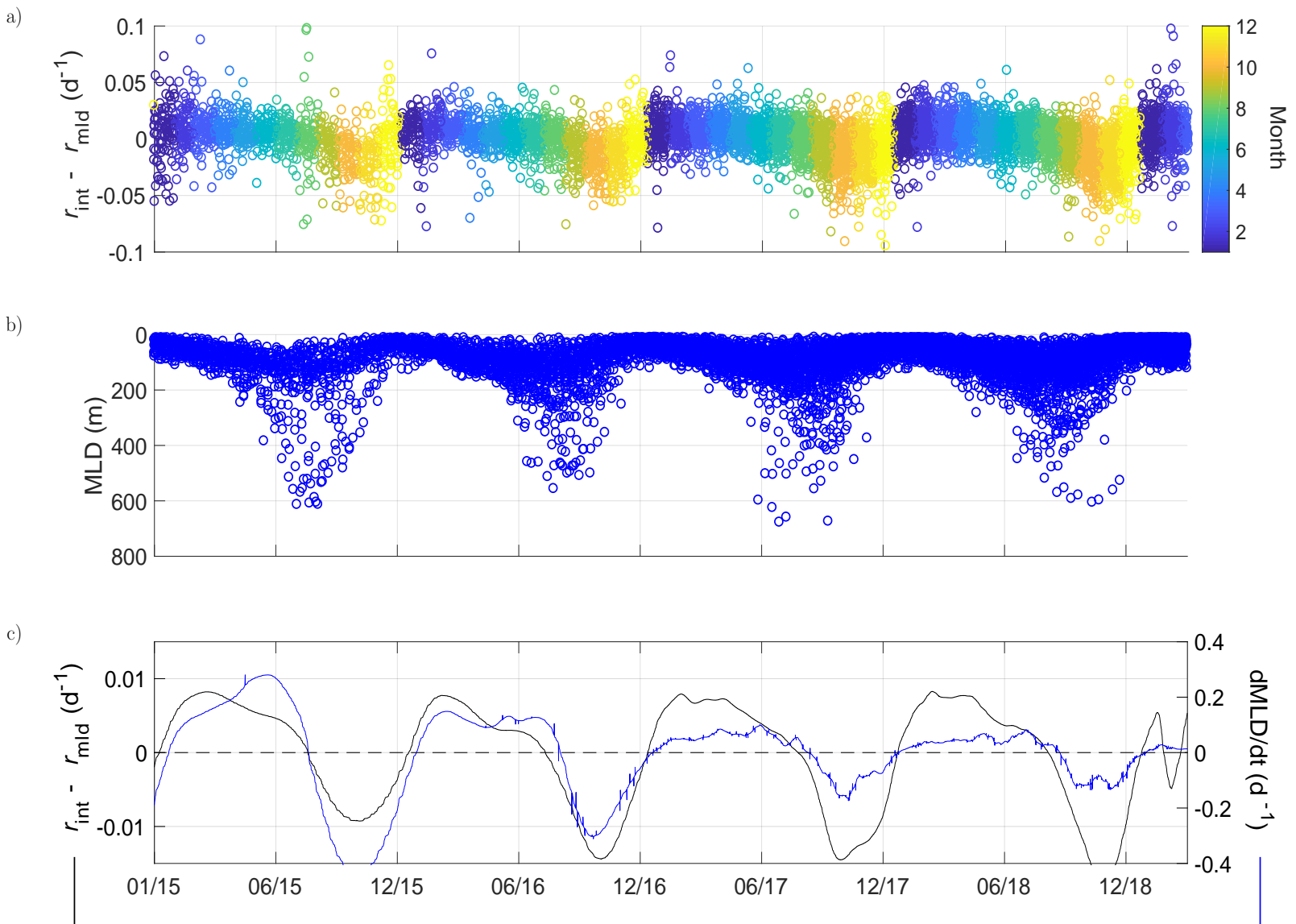
a)

b)

c)

Figure S5: (a) Difference between mean and integrated estimates of the net accumulation rate of phytoplankton biomass (r_{int} - r_{mld}). (b) Individual float-based estimates of mixed layer depth (MLD) based on in situ temperature and salinity profiles[6]. (c) Comparison between smoothed time series of r_{int} - r_{mld} (black continuous line) and the temporal derivative of the mixed layer depth (dMLD/dt) (blue continuous line).
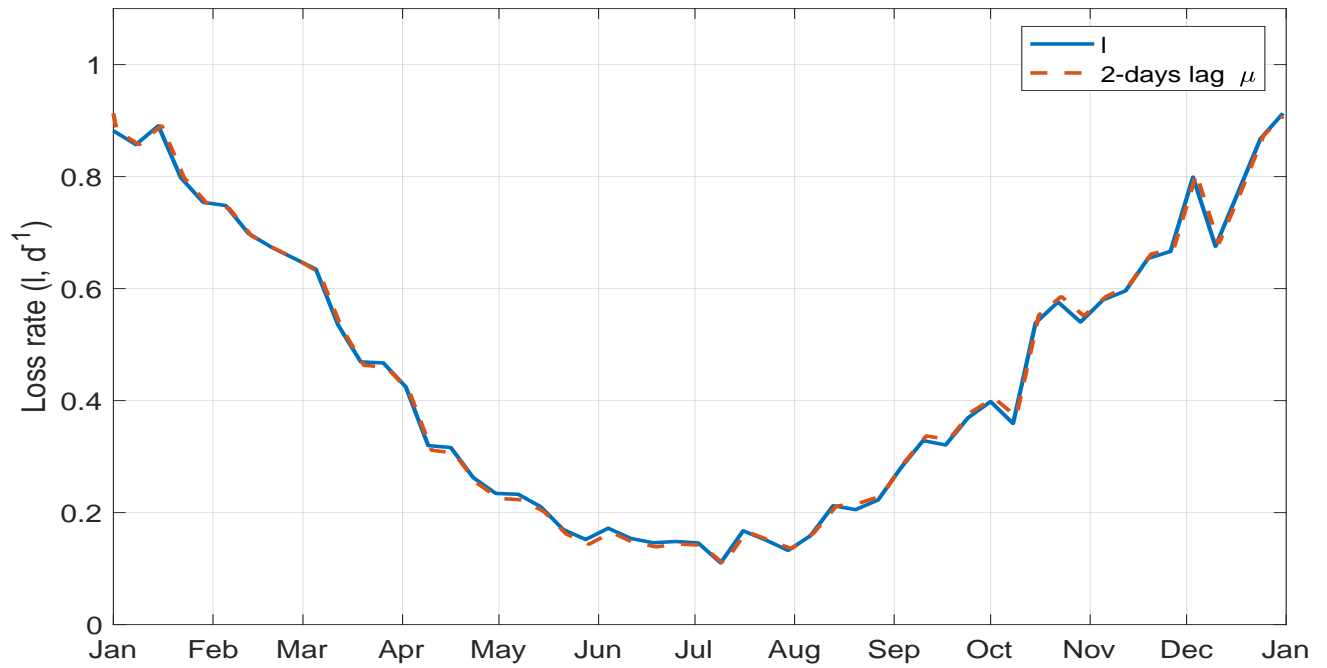
Figure S6: Climatological loss rate (l, blue line) for the Southern Ocean computed from the float-based accumulation and division rate as $l = \mu$ - r. Red dashed-line shows a reconstruction of l as 2-days temporally lagged μ.
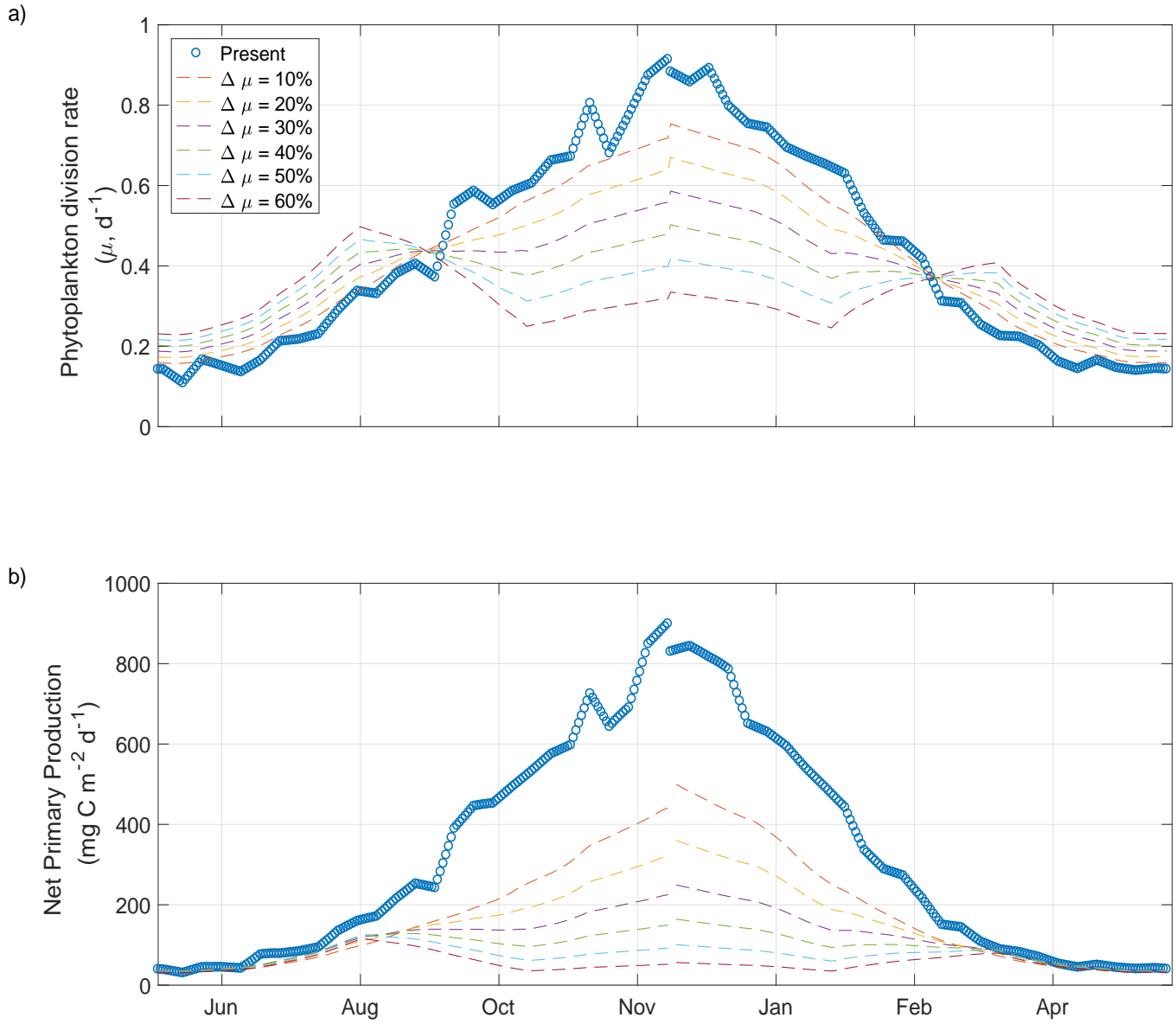
a)

b)

Figure S7: (a) Induced changes in the annual cycle of phytoplankton division rates (μ). (b) Variations in the annual cycle of vertically integrated net primary production (NPP) in the Southern Ocean resulting from relative changes in μ.

References

1. Tagliabue, A. *et al.* A global compilation of dissolved iron measurements: focus on distributions and processes in the southern ocean. *Biogeosciences* **9**, 2333–2349 (2012). URL https://www.biogeosciences.net/9/2333/2012/.

2. Boss, E. & Behrenfeld, M. In situ evaluation of the initiation of the North Atlantic phytoplankton bloom. *Geophysical Research Letters* **37** (2010). URL http://dx.doi.org/10.1029/2010GL044174. L18603.

3. Behrenfeld, M. J., Doney, S. C., Lima, I., Boss, E. S. & Siegel, D. A. Reply to a comment by stephen m. chiswell on: annual cycles of ecological disturbance and recovery underlying the subarctic atlantic spring plankton bloom by m. j. behrenfeld et al. (2013). *Global Biogeochemical Cycles* **27**, 1294–1296 (2013). URL https://agupubs.onlinelibrary.wiley.com/doi/abs/10.1002/2013GB004720. https://agupubs.onlinelibrary.wiley.com/doi/pdf/10.1002/2013GB004720.

4. Behrenfeld, M. J. & Boss, E. S. Student's tutorial on bloom hypotheses in the context of phytoplankton annual cycles. *Global Change Biology* **24**, 55–77 (2018). URL https://onlinelibrary.wiley.com/doi/abs/10.1111/gcb.13858. https://onlinelibrary.wiley.com/doi/pdf/10.1111/gcb.13858.

5. Westberry, T., Behrenfeld, M. J., Siegel, D. A. & Boss, E. Carbon-based primary productivity modeling with vertically resolved photoacclimation. *Global Biogeochemical Cycles* **22**, GB2024 (2008).

6. de Boyer Montégut, C., Madec, G., Fischer, A. S., Lazar, A. & Iudicone, D. Mixed layer depth over the global ocean: An examination of profile data and a profile-based climatology. *Journal of Geophysical Research: Oceans* **109** (2004). URL http://dx.doi.org/10.1029/2004JC002378. C12003.